Raspberry Pi Reflector (RPR): a Low-cost Water-level Monitoring System based on GNSS Interferometric Reflectometry

Makan A. Karegar[1*], Jürgen Kusche[1], Felipe Geremia-Nievinski[2], Kristine M. Larson[3]

[1] Institute of Geodesy and Geoinformation, University of Bonn, Bonn, Germany
[2]Department of Geodesy and Postgraduate Program in Remote Sensing, Federal University of Rio Grande do Sul, Porto Alegre, Brazil
[3]Aerospace Engineering Sciences, University of Colorado, Boulder, USA

[*]Corresponding author: Makan A. Karegar (karegar@uni-bonn.de)

Key Points:

- We present a prototype system for tracking water levels called the Raspberry Pi Reflector with centimeter level accuracy
- It consists of cost-effective single-frequency Global Positioning System module and navigation antenna connected to Raspberry Pi microcomputer
- It uses Interferometric Reflectometry technique and can be operated safely in extreme weather with lower operational costs

Abstract

Although reflectometry had not been considered as a primary application of GPS and similar Global Navigation Satellite Systems (GNSS), fast-growing GNSS tracking networks has led to the emergence of GNSS interferometric reflectometry technique for monitoring surface changes such as water level. However, geodetic GNSS instruments are expensive, which is a limiting factor for their prompt and more widespread deployment as a dedicated environmental sensing technique. We present a prototype called Raspberry Pi Reflector (RPR) that includes a low-cost and low-maintenance single-frequency GPS module and a navigation antenna connected to an inexpensive Raspberry Pi microcomputer. A unit has been successfully operating for almost two years since March 2020 in Wesel (Germany) next to the Rhine river. Sub-daily and daily water levels are retrieved using spectral analysis of reflection data. The river level measurements from RPR are compared with a co-located river gauge. We find an RMSE of 7.6 cm in sub-daily estimates and 6 cm in daily means of river level. In August 2021, we changed the antenna orientation from upright to sideways facing the river. The RMSE dropped to 3 cm (sub-daily) and 1.5 cm (daily) with the new orientation. While satellite radar altimetry techniques have been utilized to monitor water levels with global coverage, their measurements are associated with moderate uncertainties and temporal resolution. Therefore, such low-cost and high-precision instruments can be paired with satellite data for calibrating, validating and modeling purposes. These instruments are financially (< US$ 150) and technically accessible worldwide.

1 Introduction

1.1 Background

One of the challenges for hydrologists and environmental scientists is the need to obtain and sustain *in-situ* water level measurements for calibrating and improving models, validating satellite and airborne products, and developing early-warning flood systems. Ground-based measurements are still scarce in many regions. In particular, stream flow monitoring gauges have been declining sharply since the mid 1980s due to high maintenance cost, funding shortfall and (geo-) political constraints (Hannah et al., 2011; Ruhi et al., 2016, 2018; Reid et al., 2019). While satellite remote sensing techniques have been utilizing to monitor oceanic and land surface water with unprecedented global coverage, their measurements are associated with moderate uncertainties and temporal resolution. Measurements of sea surface and river water level using ground-based sensors are conventionally relying on contact methods, such as traditional float and stilling well gauges (Noye, 1974) and bubbler pressure gauges (Pugh, 1972), or proximal sensing gauges, such as acoustic (Gill & Mero, 1990; Boon & Brubaker, 2008) and radar sensors (Woodworth & Smith, 2003; Costa et al., 2006). These commercial sensors are typically costly at approximately a range of few hundreds (e.g., pressure gauge) to a few thousands of U.S. dollars (e.g., radar sensors). Their installations are often restricted to a specific structure close to the river such as a stilling well, a mast or a bridge. However, recent advances in commutation technology, open-source hardware, microcontrollers and single-board computers such as Internet-of-Things, Raspberry Pi computers, and GPS chipsets are transforming scientific data collection, offering a new way forward on the use of low-cost sensors for environmental monitoring.

Open-source do-it-yourself sensors can vastly reduce acquisition costs – which is a major barrier to collecting *in situ* water level data. In recent years, the use of inexpensive sensors has gained popularity in surface water monitoring and has shown great promise (e.g., Mao et al., 2020; Knight et al., 2020). Paul et al. (2020) developed a cost efficient lidar-based distance sensing prototype to monitor river water level (< $150 U.S. dollars) which has accuracy inversely proportional to distance, of about 1 cm for measurement distances below 10 m under operating temperatures of 10°-30° C. Inexpensive pressure sensors such as MS5803 have been recently combined with low-cost Arduino microcontrollers to provide sea-level data (Beddows et al., 2018; Lyman et al., 2020). Knight et al. (2021) showed that while these pressure sensors can resolve water elevations to 1 cm accuracy in laboratory settings, the effect of large waves during high water fluctuations and storms can significantly reduce the quality of water level measurements.

Water level can also be measured directly by means of buoys and gliders equipped with GPS and similar Global Navigation Satellite Systems (GNSS) instruments. Using a low-cost GNSS receiver (U-blox M8T) and a patch antenna (Tallysman TW4721) on a buoy, Knight et al. (2020) designed a unit to measure sea level with RMSE of 1.4 cm compared to a conventional tide gauge. This real-time kinematic (RTK) positioning method requires a coastal GNSS base station at a known fixed location to allow observations relative to the moving receiver on buoy; this is likely a significant limiting factor for adoption of this method. Penna et al. (2018) demonstrated a GNSS glider based on Precise Point Positioning (PPP), which does not require a base station. A more serious issue to these contact methods (pressure gauges and GNSS floats) concerns safety and sustainable monitoring due to direct exposure to the water.

1.2 GNSS Interferometric Reflectometry for Water Level Measurements

GNSS Interferometric Reflectometry (GNSS-IR) is an emerging technique in geodesy that has shown remarkable contributions to ground-based sea and lake level monitoring (Larson et al., 2013b; Roussel et al., 2015; Strandberg et al., 2016; Geremia-Nievinski et al., 2020; Holden & Larson, 2021). Although GNSS-IR is not the primary application of GPS/GNSS (positioning, navigation and timing), the fast growth of GPS/GNSS base station networks has led to the emergence of this technique for monitoring surface changes such as sea and river level. Unlike GNSS positioning applications that rely on carrier phase and pseudorange observables, GNSS-IR is based on Signal-to-Noise Ratio (SNR) data recorded by the receiver. Geodetic-quality GNSS receivers and antennas, however, are still very expensive instruments (>$10,000), a limiting factor for use as a dedicated environmental sensor. While several low-cost GNSS-IR sensors are now available (see below for further details), they typically work best in coastal ocean regions and lakes where satellite signals are reflected off a relatively large extent of water body. A river is a more challenging environment for measuring water level because of the need to restrict observations over a much narrower region.

GNSS-IR is redefining its role as an innovative technology in environmental sensing. Williams et al. (2020) demonstrated the potential of a low-priced GPS receiver ($30 U.S. dollars) for tides and sea level measurements. They mounted a GPS antenna sideways on a radio tower mast at 16 m elevation in a coastal site in Ireland and collected SNR data for about three months in 2019 over a relatively large azimuth interval 110°-251°. An XBee wireless telemetry system was used for short range data transfer from the mast to the computer inside the building. Their final unit cost was ~ $500 U.S. dollars. They reported an RMS difference of 1.7 cm relative to a nearby tide gauge at daily resolution, and an RMS of 5.7 cm over a tidal range exceeding 3 m at spring tides sub-daily. Using an upright antenna and a low-cost GPS receiver (~ $25 U.S. dollars), Fagundes et al. (2021) acquired SNR data next to the Guaíba Lake (Brazil) for approximately one year starting in 2018. They also used a wide azimuth mask (between 190° and 10°) over the lake, and a relatively short antenna mount (~ 3.5 m). They reported the daily averages of water level between the GNSS-IR and a nearby gauge to be in agreement at the 2.9-cm RMS level. Their unit total cost, including solar power, was ~ $200 U.S. dollars. Purnell et al. (2021) employed a stack of side-facing low-cost single-frequency multi-GNSS receivers (total cost ~ $200-300 U.S. dollars including solar panel and battery) to track GPS, GLONASS and Galileo satellites. The water surface reflections extended more than 140° in azimuth and over a range of elevation angles up to 50°. Collecting a few weeks of SNR data at three sites along the Saint Lawrence River in Quebec (Canada) and along the Hudson River in New York (USA), they show a range of 0.7 cm–1.2 cm for RMS of difference between water measurement from GNSS-IR sites and nearby tide gauges.

The initial GNSS-IR studies used a single zenith-pointing geodetic antenna designed to suppress reflections (Larson et al., 2013a, Lofgren et al. 2014). These sites have the advantage of sharing multiple uses (i.e. positioning and reflectometry). They can also observe multiple GNSS constellations and carrier frequencies. However, as noted, they are expensive and ultimately not as precise as a custom-designed GNSS-IR sensor. The latter can be achieved by orienting the antenna towards the water body (generally 90 degrees from zenith; Santamaría-Gomez & Watson, 2017) and/or by using an inexpensive (navigation non-geodetic) antenna (Williams et al., 2020; Fagundes et al., 2021; Purnell et al., 2021). Such installations have far superior reflection characteristics at the cost of poor positioning capabilities.

Real-time GNSS observation can provide a range of future opportunities for hydrological monitoring using low-priced receivers that can be operated unattended for a long period. Thus, it is beneficial to provide real-time or near real-time transmission of data from the sensor to a remote centralized data storage and processing server. This is especially for important for remote or risky environments, or during extreme weather events such as floods, storm surges, and tsunamis when rapid response and possible evacuation is needed. Beside remote data streaming, such telemetry capability allows a supervised remote control of GNSS unit, i.e., uploading of commands to the sensor for maintenance and upgrade. Nevertheless, because of very recent implementation of these low-cost GNSS units in surface water level monitoring, there is still room for improvement, particularly with regards to remote telemetry and real time applications. Moreover, there is still a lack of information concerning their long-term performance.

We present a prototype called Raspberry Pi Reflector (RPR) that includes a low-priced and low-maintenance single-frequency GPS module and a GPS navigation antenna connected to an inexpensive Raspberry Pi computer and a cellular modem. The system enables real-time access to SNR data and remote supervision and maintenance of GPS electronics and software. RPR builds on an earlier GNSS-IR development by adding telemetry capabilities to the offline Multipath Hardware sensor (Fagundes et al., 2021). A unit has been successfully operating for almost two years since March 2020 in Wesel (Germany) at a river gauge next to the Rhine river. The GNSS antenna was mounted at approximately 12.5 m from the river level on a steel mast tied to the gauge building. The majority of data were collected with an antenna setup in zenith direction. To quantify the impact of antenna orientation, the antenna was mounted sideways toward the river in August 2021. Sub-daily and daily water levels are retrieved using the *gnssrefl* Python software package (Larson, 2021). The accuracy of water level retrieval from GNSS-IR technique using RPR for this site is demonstrated by comparisons of sub-daily and daily water level retrievals with data from a classical float gauge.

2 Instrumentation

2.1 Hardware and Electronics

The RPR unit consists of two main subsystems: i) GNSS-IR sensor ii) Raspberry Pi microcomputer (Table 1 and Figure 1).

2.1.1 Legacy GNSS-IR Sensor (MPHW)

The GNSS-IR sensor is based on the successful Multipath Hardware (MPHW) implementation that Fagundes et al. (2021) designed and demonstrated to monitor lake water level in Brazil. In its turn, the MPHW is based on the Free-Standing Receiver of Snow Depth (FROS-D; Adams et al., 2013). The MPHW includes a single-frequency L1 (1.575 GHz) Coarse/Acquisition code (C/A) chipset (MediaTek MT3339) mounted on an Adafruit GPS FeatherWing daughterboard, capable of tracking up to 22 satellites. MPHW also uses an external Right Hand Circular Polarized (RHCP) 28-dB Chang Hong active antenna with an Ingress Protection (IP) rating 66 enclosure which is waterproof against hose-directed water, rain or snow. The GPS board is stacked to an Adafruit Feather Adalogger mainboard based on the ATmega32u4 microcontroller. The microcontroller board is the intermediate layer between the GPS board and the Raspberry Pi microcomputer. It sends out configuration and data collection commands to the GPS board and streams the GPS data tracked by the receiver to Raspberry Pi. Both data and power are transmitted via a micro-USB cable. The MPHW GNSS-IR sensor outlined in Table 1 and Figure 1 housed inside a IP66/67 weatherproof enclosure. The hardware outputs GPS SNR data in National Marine Electronics Association (NMEA) 0183 format. NMEA 0183 is one of GNSS standard protocols for real time position, velocity, time and SNR exchange with GNSS receivers. The NMEA protocol uses a plain text encoded in ASCII and contains 19 interpreted sentences for each epoch. Instructions for building the GNSS-IR sensor are provided in the supplementary information (Text S1). For the factory default Adafruit GPS FeatherWing board, SNR data are recorded with 1-dB resolution which degrades the ability to estimate reflection parameters, especially at higher elevation angles (Larson & Nievinski, 2013). We used MPHW's updated GPS firmware (Fagundes et al., 2021; Adams et al., 2013) to generate the SNR data with 0.1-dB resolution (see Text S1). Satellite azimuth and elevation angles are provided as integer values.

2.1.2 Raspberry Pi

Open-source sensors in environmental monitoring are increasingly being built upon the Raspberry Pi microcomputers. Raspberry Shake, a low-cost seismograph, serves as a leading example that has demonstrated the capability of Raspberry Pi for long-term motioning (https://raspberryshake.org/). Some recent field applications include observing carbon dioxide concentrations (Martin et al., 2017), and ionospheric irregularities (Rodrigues & Moraes, 2019). The Raspberry Pi (https://www.cl.cam.ac.uk/projects/raspberrypi/), released in 2012, is an easy-to-use, low-power, single-board tiny microcomputer that includes main input/output and Ethernet ports, and supports open source operating systems including Linux and Raspbian. It can be used like a personal laptop as a fully functional computer, enabling storage, analysis and visualization of data with a vast variety of third-party packages available. We used Raspberry Pi 4 Model B with 2 GB RAM and 64-bit quad core processor running at 1.5GHz. We used a built-in heat sink and a thermal pad which allows transferring heat between the Raspberry Pi's CPU and the housing case and ensure functionality of Pi computer in outdoor summer temperature. Given the limited storage space on the Raspberry Pi and real time applications, we set up an external server through SSH (Secure SHell) network protocol to communicate with the Raspberry Pi microcomputer and MPHW GNSS-IR sensor. Internet connectivity can be achieved via an Ethernet/LAN cable, via Wifi or an USB dongle (cellular modem). We used an LTE dongle (Huawei E3372 4G/LTE modem) which supports LTE download and the Raspberry Pi operation system. The Huawei E3372 dongle comes with a connector for an external antenna for better signal reception from a local internet service provider, which was not used.

The current system works with an AC/DC adapter, for particularly accessible utility power supply environments. However, the RPR can use a solar panel instead of a power supply by connecting the Raspberry Pi to a solar panel battery system.

Table 1. Off-the-shelf components of the Raspberry Pi Reflector (RPR). Costs are accurate as of November 2021. The main hardware is illustrated in Figure 1.

subsystem	component	function	version	source	price (USD)
Raspberry Pi (RP)	Raspberry Pi	uploading commands to GPS, data transfer	4, Model B, 2GB RAM	www.raspberrypi.org	$35
	Raspberry Pi plug-in power	power supply	15.3W USB-C	www.raspberrypi.org	$8
	Heat sink pack	built-in heat sink	FIT0542	https://www.digikey.com	$1.29
GNSS-IR sensor	Adafruit GPS FeatherWing	a single-frequency GPS L1 C/A receiver	Ultimate, MediaTek MT3339	https://www.adafruit.com/product/3133	$24.95
	Adafruit Feather Adalogger	microcontroller to interface GPS and RP	32u4	www.adafruit.com/product/2795	$21.95
	Chang Hong GNSS antenna	external active antenna, 3-5V and 28 dB	Chang Hong GPS-01-174-1M-0102	https://www.adafruit.com/product/960	$17.95
	Fibox polycarbonate housing	IP66/67 weatherproof housing	Dimension: 180 x 130 x 75 mm	https://de.rs-online.com/	$24
additional components	micro SD card	disk storage for RP	16 -128 GB	www.amazon.com	$8.5
	SMA to RF adapter cable	for connecting the antenna to GPS board	-	www.adafruit.com/product/851	$3.95
	USB to mini USB plug cable	For connecting the RP to the microcontroller	-	www.amazon.com	$6.71

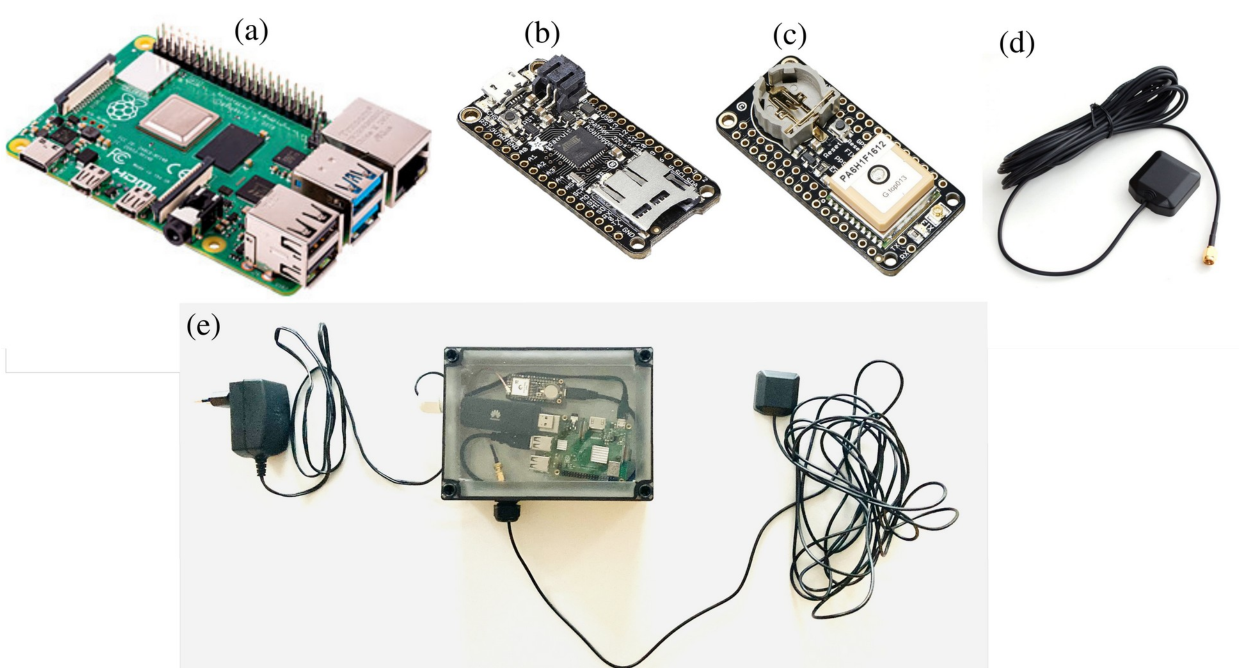

Figure 1. The RPR hardware array comprising: (a) Raspberry Pi 4 Model B (b) Adafruit Feather Adalogger microcontroller (c) Adafruit GPS FeatherWing receiver (d) GPS external antenna (e) Configuration of RPR prototype setup used. This setup uses 4G/LTE dongle modem.

2.2 Software

Three layers of software programs are utilized to retrieve water levels from the RPR. The first layer is based on the Arduino Integrated Development Environment (IDE), which is used to configure, set up and communicate with GPS module. The second layer is made of embedded Python codes, which initiates the RPR, enables acquiring GPS data and storing in a text file, and updates the RPR's clock. And the last layer is the *gnssrefl* open source Python software package, which is used for retrieving water level from SNR data (Larson, 2021).

2.2.1 Arduino IDE

The 32u4 microcontroller is programmed via the Arduino IDE, a simple platform based on the C/C++ language that provides a user-friendly interface. Arduino IDE enables writing, compiling and uploading programs (often called "sketches") from a personal computer (e.g., the Raspberry Pi) to the microcontroler board via a USB cable. The Arduino IDE can support third-party boards such as Adafruit's via the Additional Boards Manager URLs option (see Text S2 in supplementary information). We adopted the original MPHW sketch written by Fagundes et al. (2021) to configure the GPS sensor and print the GPS data characters (in NMEA format) via a serial event. We modified the sketch to stream only GPS data to a serial port instead of writing to an SD card to interact with the Raspberry Pi via our Python codes (explained below). This sketch includes two main parts: a "Setup" and "Loop". The "Setup" part establishes serial communication between the GPS module and the Raspberry Pi computer via a USB cable, configures GPS settings (e.g., GPS sampling rate) and allocates a string variable to store the encoded GPS data. The "Loop" part keeps buffering the GPS characters in a string and streams them to the serial port.

2.2.2 Embedded Python Codes

We provide Python code (`dataPicker.py`) to directly read each serial event from the Raspberry Pi serial port and write them to a text file. We use the `pySerial` library to access the serial port communication in Python. The GPS NMEA 0183 strings are written and stored as data files on the Raspberry Pi. The Python code `dataPicker.py` instruct the RPR to archive daily data files for batch post-processing in the *gnssrefl* software.

Unlike standard computers, the Raspberry Pi microcomputer does not include a built-in real-time clock. Its clock is synchronized via WiFi or Ethernet connection and keeps its time and date by checking the internet network. However, network issue can occur, especially when using USB dongle and thus time may not kept during connection break. We experienced network issues from August 21 to 31, 2020 and from March 17 to 23, 2021. Since the Raspberry Pi could not synchronize its clock, RPR data were lost. We solved this issue by providing a second embedded Python code (`setPiClock.py`) to keep the RPR clock updated using NMEA data transmitted from the GPS module.

We automate data picking and Raspberry Pi's clock synchronization by setting up two boot-based cron jobs that run these python codes whenever the Raspberry Pi boots up (see Supporting Information Text S1).

2.2.3 Post-processing Python Codes (*gnssrefl*)

Our RPR data are post-processed using *gnssrefl* open-source Python software package (Larson, 2021). Designed specifically for ground-based GNSS-IR applications, *gnssrefl* allows for data download from global GNSS archives, format conversion, data assessment, core processing, as well as producing daily or sub-daily reflector height. It provides support for RINEX (Receiver Independent Exchange Format) versions 2.11 and 3 as well as NMEA (NMEA, 2018). These data files are translated and the SNR observations are extracted along with the time stamp and satellite azimuth and elevation angles. Tools are available online (https://gnss-reflections.org/rzones) to help the user visualize the reflection points and Fresnel zones near a GNSS site. Although *gnssrefl* can analyze signals from all constellations, only GPS L1 signals are used in this study. *gnssrefl* analyzes all rising and setting satellite arcs from the user-defined azimuth and elevation angle range. The dominant SNR frequencies are extracted using a Lomb-Scargle periodogram (LSP) and converted to reflector heights (see section SNR data processing for details).

3 Test Site and Data Acquisition

To assess the long-term performance of RPR and the accuracy of its water level estimates, we deployed a unit within 7 m distance to a continuously operating river gauge on the Rhine river in Wesel, Germany. In March 2021, the RPR antenna was mounted about 13 m above the ground surface in order to maximize the reflection zone while also keeping the antenna and electronics safely above the water surface in all anticipated river levels. We fixed the antenna on a vertically oriented steel pipe and then securely tightened the pipe to the gauge house's railing (Figure 2). The RPR electronic cases were placed inside the river gauge’s building for power access. The RPR collects SNR data every 1 second for all available GPS satellites and streams the data every two hours to a remote server for archiving and processing.

The river width at our test site is ~200 m when there is no drying out at very low water during extreme drought periods. The 13-m antenna height above the river surface allows sensing of the first Fresnel zone with maximum dimensions of 10 m by 190 m corresponding to satellite elevation angles ranging between 5° and 30° for each satellite ground tracks. Thus, the water surface is fully sensed from one side to the other. However, there is a bridge to the north of the antenna which interferes with the reflected signals. We imposed an azimuth mask to limit the reflection data to the river surface next to the RPR antenna (Figure 2c). In August 20 (2021), we changed the antenna orientation setup, from zenith-pointing to sideways facing the river surface towards the masked reflection zone. We assess the effect of such modification in our data analysis.

The river gauge in Wesel, maintaining by German Federal Waterways and Shipping Administration (WSV), records water level at 15 minutes intervals. It is a classical float and stilling well gauge sitting on the river bank and connected to the water via an underground pipe. The accuracy of the river gauge records is thought to be ~3 cm (personal communication, WSV technician). Stilling wells act as a mechanical low-pass filter, so the hourly bands suffer some attenuation and lagging (IOC, 2006). The level of this section of the Rhine river is rainfall-dominated. Discharge is high during winter and low during summer (Figure S1a). Flooding often occurs in winter from rainfall. However, the heavy rainfall in July 2021 led to severe flooding in Western Europe including the Rhine river. A wind sensor, operated by the German Weather Service, is located in Xanten, 12.5 km from the Wesel sensors; it measures the wind speed at hourly intervals about 10 m above the ground.

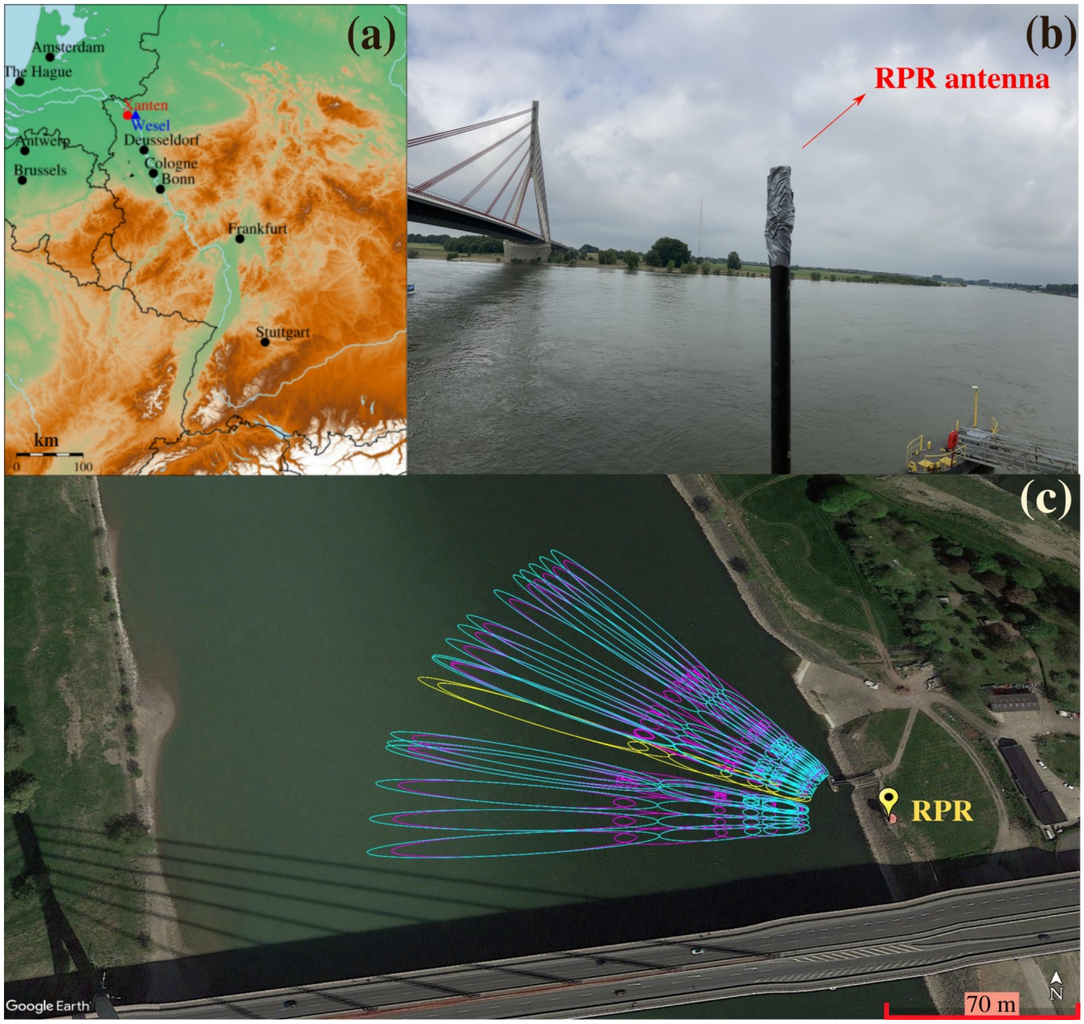

Figure 2. **(a)** Location and field setup of the RPR antenna in Wesel, Germany. **(b)** The GPS antenna is mounted on a steel pipe, upright-pointing from March 23 (2020) to August 20 (2021) and sideways since then. The RPR electronics are housed inside the river gauge's building. **(c)** Footprints of the reflected GPS signals projected on a Google Earth image. Ellipses are first Fresnel zones corresponding to azimuth 265° - 330° for RPR antenna, respectively. Yellow ellipses show first Fresnel zones for GPS satellite with PRN 16. Signal-to-noise ratio (SNR) data on L1 C/A data for this satellite are shown in Figure 3.

4 SNR Data Processing

As it is not meant for geodetic applications, satellite elevation and azimuth angles are only integer values in the NMEA format. Since they follow a very smooth but discrete trend, the decimal parts can be restored by linear interpolation through a de-quantization process in the `nmea2snr` module of *gnssrefl*. The main observable of GNSS-IR is based on the constructive and destructive interference between the direct and reflected GNSS signals (Figure 3a). The latter always travels a longer distance than the direct signal. For a horizontal and planar reflection (such as a river surface), this interference pattern yields periodic oscillations in SNR data (Figure 3b). The frequency of the oscillations primarily depends on the wavelength of the carrier wave transmitted by satellites (a constant known *a priori*) and the vertical distance between the antenna phase center and the reflecting surface, which is the unknown of interest, termed the reflector height (Larson et al., 2009). The direct signal effect needs to be removed by fitting a low-order polynomial to the SNR measurements. Power spectral density analysis is used to determine the dominant SNR frequency and thus the reflector height. Details of the theoretical principles and methods underlying SNR-based GNSS-IR may be found in the literature (Nievinski & Larson, 2014; Roesler & Larson, 2018) as well as the *gnssrefl* software description (Larson, 2021).

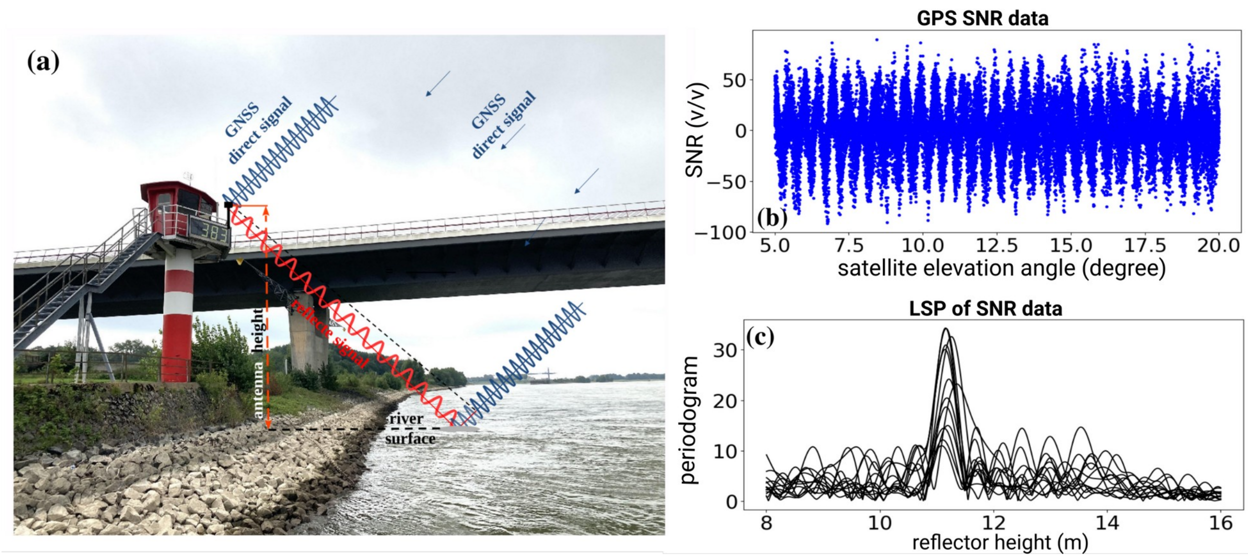

Figure 3. (a) GNSS Interferometric Reflectometry (GNSS-IR) geometry for a horizontal planar reflector. A GNSS antenna measures the interference between the direct (blue) and reflected (red) signals. **(b)** Signal-to-noise ratio (SNR) data on the L1 frequency as a function of satellite elevation angle for all GPS satellite tracks with an azimuth between 265° and 330°. These oscillation patterns in SNR data represent reflected signals. **(c)** Spectral analysis of the SNR data in b). Peaks in the periodograms corresponds to the estimated reflector heights for each satellite arc.

We imposed azimuth (265° and 330°) and elevation angle (5° and 20°) masks to isolate the reflections to the river surface (Figure 2c). The first Fresnel zone is the ellipse located along each satellite ground track (Larson & Nievinski, 2013). It represents the footprint of reflected signal. It mainly depends on reflector height (Figure 3a). In addition to the site-specific masks, the *gnssrefl* software also allows the user to parameterize other inputs. For completeness, we summarize them here. We set the noise floor in reflector height to the region between 3 m – 16 m, we require periodogram amplitudes to be larger than 8 volts/volts (see Figure 3c), the spectral peak must be 2.7 larger than the noise, and each arc cannot last longer than 1 hour. We use a quantity called sub-daily resolution (number of tracks per time period) which for the RPR setup in Wesel is 9 per day. We also averaged the sub-daily reflector heights (water level) over 24 hours to produce daily time series of water level (see section 5).

5 Water Level Results and Discussion

The RPR instrument samples raw SNR data at 1 Hz and provides continuous and real-time SNR data via cellular telecommunication networks to a host server. However, the time required to retrieve water level for each satellite arc with GNSS-IR depends on the method used for analyzing SNR data. Kalman filtering has been recently used to combine multiple simultaneous satellite arcs for real-time water-level retrieval (Strandberg et al., 2019). The LSP method requires, however, typically 20-45 minutes to retrieve a reflector height for an individual satellite arc. The retrieval time depends mainly on the elevation angle mask and the vertical distance between the GNSS antenna and the reflecting surface. At our test site ~ forty minutes on average is required for data acquisition and water level retrieval for an individual satellite track (Figure 4b).

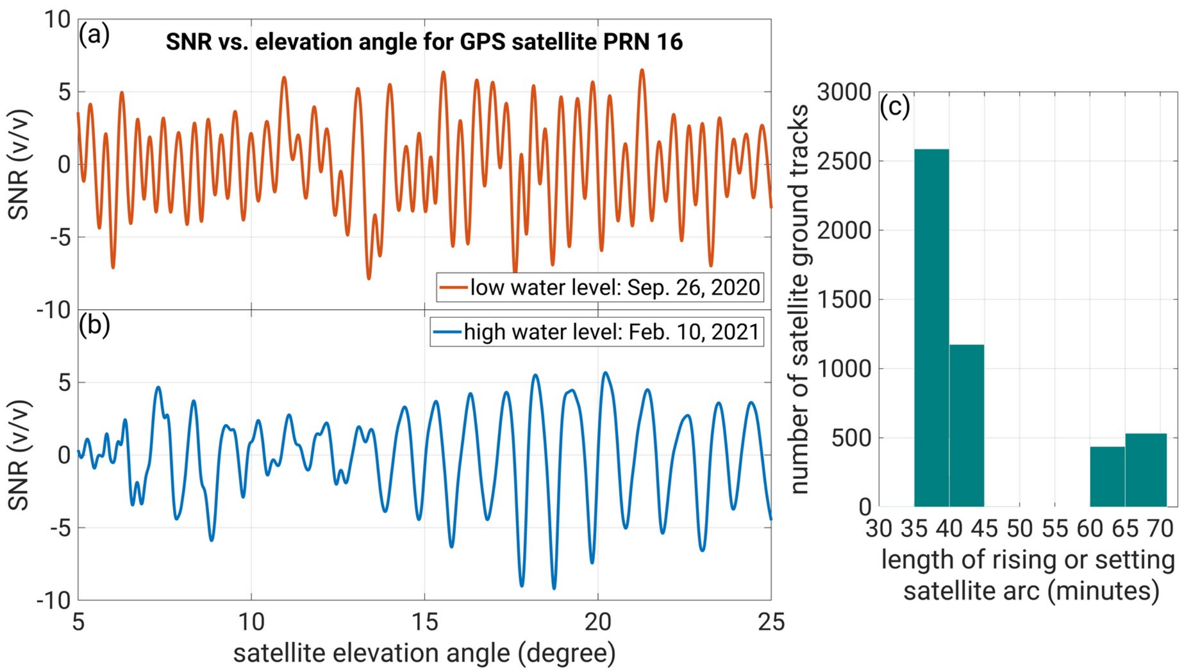

Figure 4. Detrended SNR data (after removing the direct signal) for upright RPR antenna during **(a)** low river water level (1.3 m) and **(b)** high water level (9.45 m). The SNR data oscillate at a higher frequency when the reflector height is higher (red line). The 1-second SNR data were smoothed using spline interpolant. **(c)** Histogram showing time span of rising or setting satellite arc for masked elevation angles shown in Figure 2c. It takes about 30-60 minutes that signal from a given satellite is reflecting from the river surface in our test site.

Historical data (2010-2021) for the Rhine near Wesel indicates the 80th percentile of day-to-day water-level variation amounts to 20 cm (Figure S1, panel b and c). We then identified a retrieved water-level from RPR measurements as outlier when it differed from the median value of sub-daily estimates of water level by more than 20 cm. For days with sharp water fluctuations following rainfall events and spring floods, we use linear least-squares regression to find the best fit of a linear model to each RPR sub-daily water level measures. We then identified a data point as outlier when it differs from the least squares linear model fit by more than 25 cm.

Figure 5a and 5b show sub-daily water level from RPR compared to water level from the co-located stilling well river gauge. Each RPR water level point represents an average value over the satellite descending or ascending arc. The Rhine experienced winter flooding period in mid-February followed by exceptional flood event in July 2021. Water level fluctuations during annual flooding can be substantial and reach levels of 8 m, which causes overbank flooding. The RMS of differences between two sub-daily water level time series over the entire data record is

7.6 cm. The RPR captured well diurnal variations in river level during flooding events, for example the July 2021 heavy rain induced flood event in Western Europe, as well as drought periods at low water. During July 9-16 (2021), significant rainfall sharply increased the Rhine level from 4.5 m to 8.9 m at this site. The maximum water level was observed on 16 July and then rapidly decreased. All phases of this sequence are observed accurately by the RPR. The quality of RPR sub-daily water level data is significantly improved by forming daily mean (Figure 5). The RMS of differences between two water level data reduces from 7.6 cm (sub-daily) to 6 cm (daily). Daily averaging filters out random sources or error.

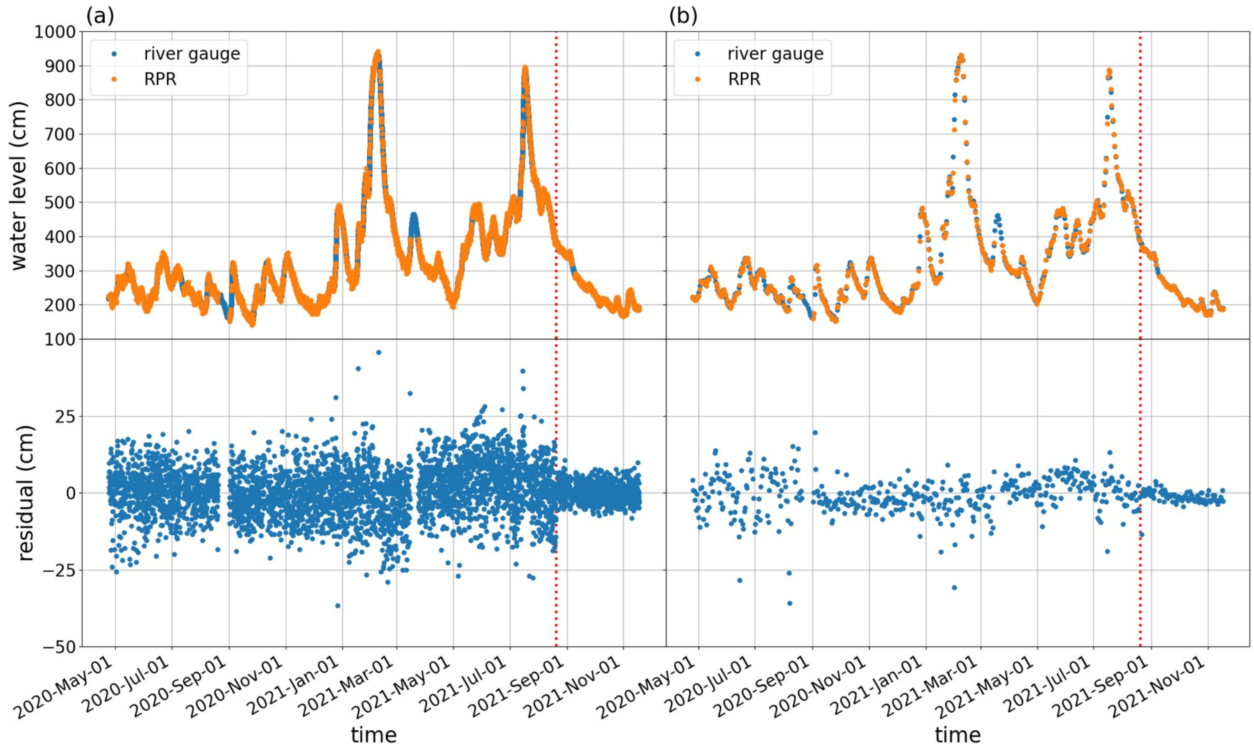

Figure 5. Water level from the river gauge and RPR. **(a)** sub-daily **(b)** daily mean. The lower panel plots are residual between the river gauge and RPR water level measurements. The vertical red dash line marks date of RPR antenna orientation change from upright to sideways. Heavy rainfall in summer 2021 (July 9-16) in Western Europe resulted in a peak at a level of about 9 m in Wesel, Germany.

5.1 Impact of Antenna Set-up Orientation

The GNSS-IR technique has primarily been used with zenith-pointing geodetic-quality GNSS instruments. Previous studies have shown that a sideways-looking antenna will improve the quality of SNR retrievals (e.g., Santamaría-Gómez & Watson, 2017). We thus set a new antenna configuration on August 20 (2021) by tilting the antenna from zenith direction to zenith angle 90° toward the river. The interference pattern recorded in SNR data from the sideways antenna are more distinct, with less noise and stronger oscillation amplitudes than data from the zenith-pointing antenna (Figure 6). The increased amplitude follows from the gain applied by the antenna to surface reflections, while the reduced noise results from the mitigation of cross-channel interference when fewer satellites are tracked. For this reason, we extended the elevation angle mask up to 30° for analyzing data recorded after the new antenna orientation setup. The improvement can be better quantified by comparing the retrieved water levels from these two datasets with the standard river gauge (Figure 5). The RMS of sub-daily residuals reduces from 7.6 cm to 3 cm for the time spans before and after the antenna orientation change. For daily residuals, the RMS decreases from 6 cm to 1.5 cm.

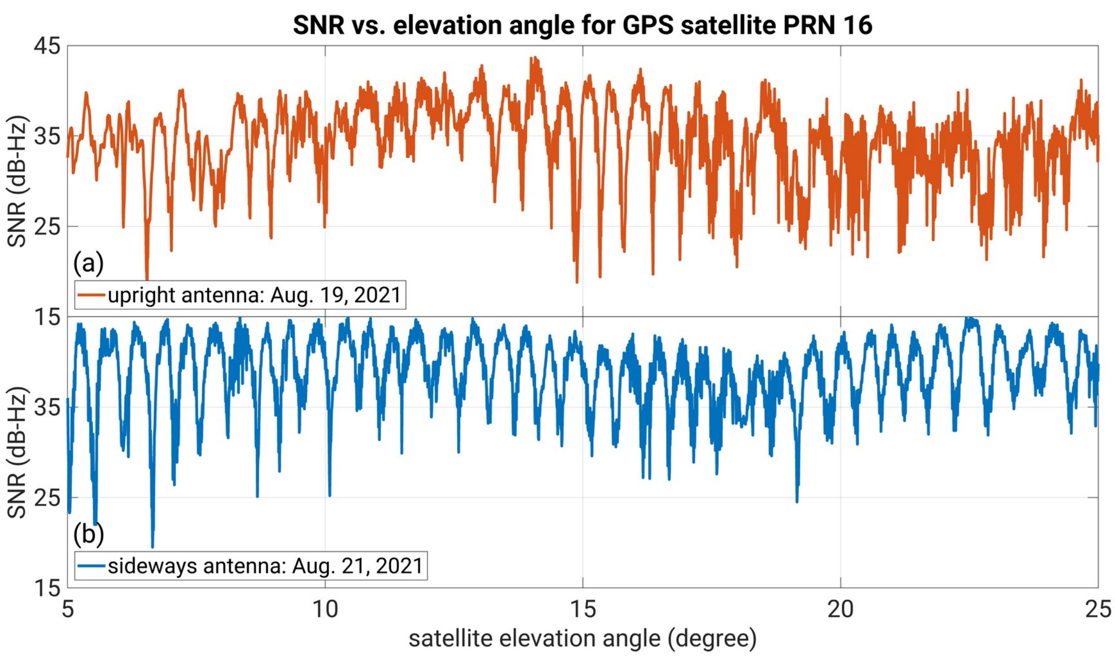

Figure 6. Examples of 1-second Signal-to-Noise Ratio (SNR) data for **(a)** upright and **(b)** sideways RPR antenna setup on August 19 and 21 (2021), respectively. The SNR data are for a GPS satellite with PRN 16, (yellow ellipses in Figure 2c).

5.2 Wind Effect

The relation between the dominant SNR frequency and reflector height (GNSS-IR reflection model) is based on the assumption of the homogeneous flat and leveled reflecting surface (Larson & Nievinski, 2013). Environmental forcing such as tide, tsunami and wind introduces surface deviations, both small-scale random roughness and large-scale systematic tilting. In their turn, roughness and tilting affect respectively the amplitude and frequency of SNR oscillation, thereby decreasing the accuracy of retrieved reflector height (e.g., Karegar & Kusche, 2020; Holden & Larson, 2021). In our study area, tides are absent. To examine the possible effect of wind, we compare the differences between sub-daily RPR and river gauge time series to hourly wind speeds. Large differences are evident during elevated windy hours (> 6 m/s) when slight roughness was generated by turbulent boils on the water surface by wind (Figure 6). Modification to the GNSS-IR reflection model has been suggested for sea level and significant wave height retrieval (e.g., Alonso-Arroyo et al., 2015; Roggenbuck et al., 2019). However, this effect is difficult to quantify for river level, in part because smaller roughness that occurs in river surface (typically smaller than 0.3 m in height). The effect of significant wave height is more likely to be notable if the wind blows along the azimuth the antenna is pointing (Reinking et al., 2019). Residuals reduce after antenna orientation change. However, the use of RPR for river level monitoring during very windy hours should be used with caution (e.g., > 6-7 m/s). For sea level or tidal river applications where high tidal current speed and/or significant wave height are expected, a modification of GNSS-IR reflection model is required.

Human-induced variations have also been shown to have a large impact on accuracy of reflector height. Karegar & Kusche (2020) showed that the coherent power of a reflecting signal from a parking lot next to a GNSS site increases with beginning of COVID-19 lockdown as the reflector surface became more planar (smoother) due to absence of cars. The Rhine river is one of the world’s busiest inland waterways where the high shipping traffic density itself (Figure S2) and waves induced by the busy traffic could also cause additional errors in retrieved water level. Such a site-specific effect requires extensive screening of shipping traffic, and it could be the subject of future research.

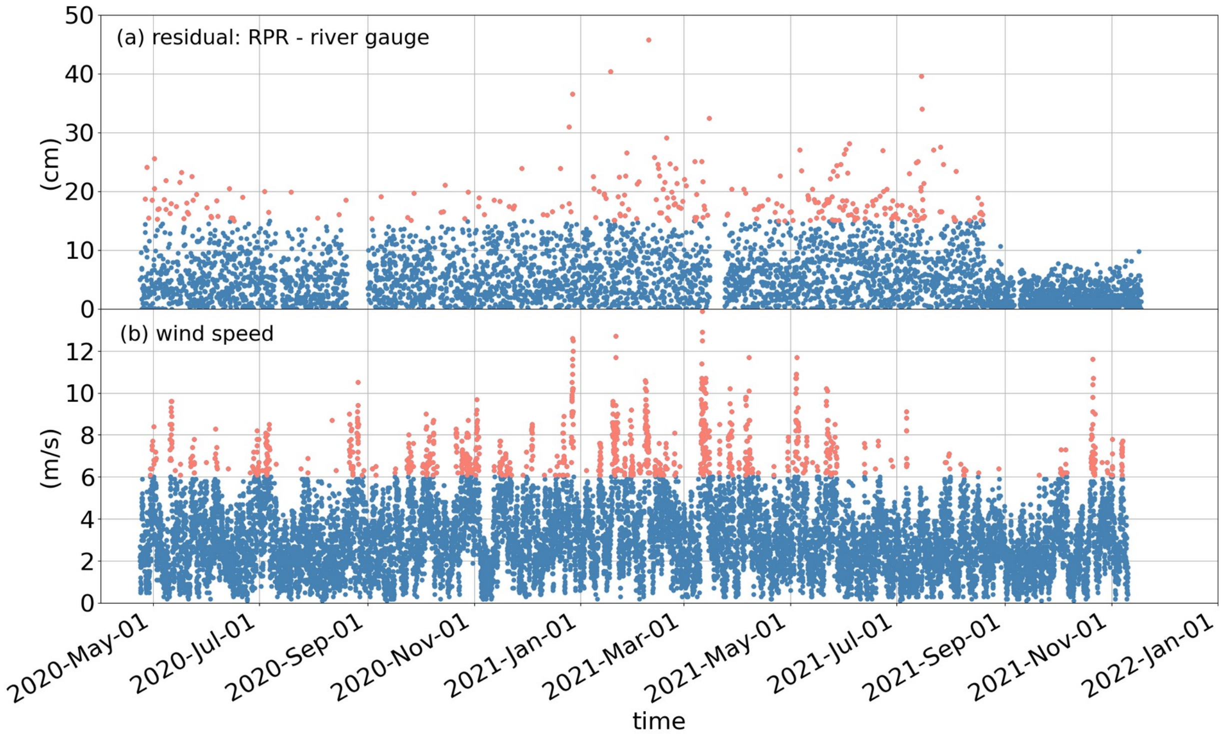

Figure 7. (a) Absolute value of water level residuals between the river gauge and RPR measurements. Residuals greater than 15 cm are shown with red dots. **(b)** Hourly wind speed measured 10 m above the ground surface at a station ~ 2.5 km from the RPR.

5.3 Limitations

The low-cost RPR instrument has the capability of long-term monitoring of water-level and can be considered as part of adaptive monitoring efforts for maintaining the integrity of long-term water level records. However, as with any monitoring technique, the RPR/GNSS-IR method has limitations. First, the GNSS-IR technique has a footprint that depends on the antenna height and satellite elevation angle. For a RPR with an antenna height of 1.5 m, its footprint would have an average radius of ~40-50 m. The footprint becomes larger as the antenna is mounted higher (e.g. ~ 200 m for a 13 meter height at Wesel). For the GNSS-IR technique to work on smaller rivers, the antenna must be carefully placed closer to the water surface, either on the banks or in a bridge. Because of the footprint issue, it would also be necessary to rotate the antenna so that higher elevation angles could be used.

5.4 Potential Application in Shallow Subsidence Measurement in Deltaic Plains

Use of the RPR instrument can also be extended to deltaic environments to quantify shallow sediment compaction. It is crucial to quantify the vertical movement of deltaic plains and identify sites at greatest risk from sea-level rise. In actively subsiding coastal plains such as river deltas and coastal alluvial plains, rapid compaction of Holocene-age (around 11,500 years before present) sediment can add a significant component to the rate of surface lowering and thus rate of relative sea-level rise. GNSS stations and tide gauges anchored in unconsolidated Holocene sediment record the contribution of compaction occurring in sediment below their anchoring depths, as well as contributions from deeper processes (e.g., Keogh & Törnqvist, 2019). However, ground surface changes related to shallow displacements that occur within the shallow layer between the surface and the base of the tide gauge or GNSS monument, often called shallow sediment compaction, is disregarded because this process has been difficult to quantify (Figure 8). Recent studies showed that the rate of shallow compaction is comparable to or larger than the rate of global sea-level rise. Thus, estimates of future flood risk and land loss in regions of rapid Holocene sedimentation may be underestimated if not accounted for (Jankowski et al., 2017; Keogh and Törnqvist, 2019; Karegar et al., 2021). Shallow compaction has been recently quantified using GNSS-IR technique at available geodetic GNSS sites in two coastal regions with thick Holocene deposits, the Mississippi Delta in North America and the eastern margin of the North Sea in Europe (Karegar et al., 2021). Since the primary aim of existing geodetic GNSS networks is tectonic geodesy and survey engineering, geodetic-quality GNSS antennas are not ideally located for purposes (i.e., close to a planar natural and preferably bare ground surface). The RPR instrument offers a low-cost, simple and high-precision method for simultaneously quantifying rate of shallow subsidence and rate of relative sea-level rise.

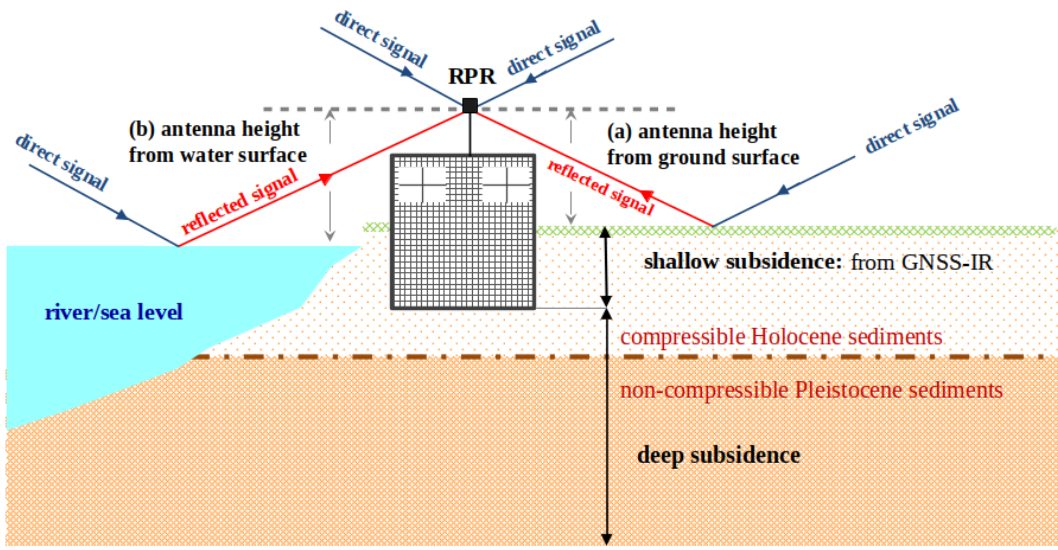

Figure 8. Schematic sketch of RPR installation in deltaic plains that measures (a) antenna height form ground surface (b) antenna height from water surface. Analysis of reflection data from ground is used for estimating shallow vertical land motion (displacements that occur within RPR's foundation structure). The compressible young Holocene age sediments are underlain by non-compressible old Pleistocene age sediments. Analysis of reflection data from the sea surface can be used to estimate relative sea-level change: the sum of absolute sea-level change and deep vertical land motion (displacements that occur beneath RPR's foundation structure).

A RPR set-up shown in Figure 8 can provide corrected rate of relative sea-level rise for the effect of shallow sediment compaction. In this configuration, the RPR antenna receives a reflected signal from the ground surface and thus the reflector height changes include the effect of ground surface changes related to shallow displacements that occur above the base of the RPR monument (building in Figure 8). The RPR also receives reflected signal from the sea surface. The reflector height changes relative to the sea level is attributed to relative sea-level change. Note that in this case, the RPR relative sea-level change measures include deep subsidence that occur beneath the structural foundation of its monument as its foundation moves relative to the sea level. However, precise geodetic-quality GNSS instrument and conventional GNSS positioning analysis is still needed if determining deep subsidence is desired. In many situations where it is desirable to estimate rate of relative sea-level rise and land loss, a dense regional network of RPR sites can be developed. This is particularly important given the need for cost-effective responses to the effects of climate change.

6. Summary and Concluding Remarks

With floods and droughts becoming increasingly frequent as climate change worsens, there is a compelling need to improve hydrological data collection. Inexpensive open-source hydrological sensors facilitate the acquisition of new *in situ* data. In particular, inexpensive novel sensors are increasingly being developed for sea level and river water monitoring. We have developed a cost-effective water level sensor called Raspberry Pi Reflector (RPR), using Global Navigation Satellite System Interferometric Reflectometry (GNSS-IR). It has been demonstrated capable of measuring river level with centimeter level accuracy. Since the GNSS-IR instrument is not in contact with the water, it can be operated safely in extreme weather with lower operational costs. Our RPR sensor streams near real-time raw data allowing continuous water level measurement. Only a single-time site visit is required for installation. The RPR consists of two main subsystems: (1) GNSS-IR sensor that includes single-frequency GPS receiver, microcontroller and external GPS antenna, and (2) Raspberry Pi microcomputer and cellular modem. We have been operating a unit on the Rhine river since March 2020 to examine the long-term performance of the RPR. The river level measurements from RPR were compared with co-located river gauge measurements. We obtained an overall accuracy of 3 cm for sub-daily water level measurement for the RPR setup with an antenna rotated 90 degrees from zenith. The RPR does not need infrastructure such as a bridge or pier for installation, and it costs less than $150 U.S. dollars. However, the RPR may not work well in narrow rivers (< ~ 50 m width) or in rivers located in steep valleys where satellite signals are blocked at low elevation angles. At our Wesel site, the unit successfully recorded flooding events associated with July 2021 flash rainfall event in western Europe and other heavy rainfall events. The RPR sensor can be applied to a variety of areas including rivers, lakes, dams and sea. It could aid stream flow estimation, and through pairs of devices along the river allows measuring river slope changes. This sensor could also be used to simultaneously quantify shallow sediment compaction in deltaic plains and monitor relative sea level change. Such potential application can provide a more complete picture of land loss and relative sea-level rise in these regions.

Acknowledgments

M. A. K. acknowledge partial funding from Austrian Science Fund (FWF) (project P30097-N29) and The University of Bonn's Argelander Starter-Kit (project 36A-40003-27-71060007), F. G. N.: National Council for Scientific and Technological Development (CNPq; grant numbers 433099/2018-6 and 310752/2019-1) and the Rio Grande do Sul State Research Funding Agency (Fapergs, grant number 17/2551-0001127-9). K. M. L.: NASA (grant number 80NSSC20K1731). We thank Jan Böhme and the German Federal Waterways and Shipping Administration for logistical support.

Open Research

RPR data processed in this study are archived at data server at the University of Bonn, Institute of Geodesy and Geoinformation (https://uni-bonn.sciebo.de/s/gQLub35odUc17eL). The wind speed data are available from the German Weather Service (DWD) ftp server https://opendata.dwd.de/climate_environment/CDC/observations_germany/climate/hourly/wind/recent). The last thirty day river gauge data in Wesel is available from the German Federal Waterways and Shipping Administration (WSV) web site (https://www.pegelonline.wsv.de/webservices/files/Wasserstand+Rohdaten/RHEIN/WESEL/). Access to the *gnssrefl* is available from GitHub (https://github.com/kristinemlarson/gnssrefl), pypi.org (https://pypi.org/project/gnssrefl), or via a Jupyter notebook implementation in a Docker image (https://www.unavco.org/gitlab/gnss_reflectometry/gnssrefl_jupyter). Guide to assemble a RPR sensor is provided in Supplement Information.

References

Adams J., Al Kaabi H., Brill S., Even R., Khan U., Miller M., Smith J., Whitney M. (2013) FROS-D: Free-Standing Receiver of Snow Depth (Aerospace Engineering Sciences Senior Design Project). University of Colorado Boulder, Department of Aerospace Engineering Sciences.

Alonso-Arroyo, A., Camps, A., Park, H., Pascual, D., Onrubia, R., & Martín, F. (2014). Retrieval of significant wave height and mean sea surface level using the GNSS-R interference pattern technique: Results from a three-month field campaign. *IEEE Transactions on Geoscience and Remote Sensing*, *53*(6), 3198-3209.

Anderson K.D. (2000) Determination of water level and tides using interferometric observations of GPS signals. *J Atmospheric Ocean Technol*, 17(8):1118–1127.

Beddows, P. A., & Mallon, E. K. (2018). Cave pearl data logger: A flexible Arduino-based logging platform for long-term monitoring in harsh environments. *Sensors*, *18*(2), 530.

Boon, J. D., & Brubaker, J. M. (2008, September). Acoustic-microwave water level sensor comparisons in an estuarine environment. In *OCEANS 2008* (pp. 1-5). IEEE.

Costa, J. E., Cheng, R. T., Haeni, F. P., Melcher, N., Spicer, K. R., Hayes, E., ... & Barrick, D. (2006). Use of radars to monitor stream discharge by noncontact methods. *Water Resources Research*, *42*(7).

Fagundes, M. A. R., Mendonça-Tinti, I., Iescheck, A. L., Akos, D. M., & Geremia-Nievinski, F. (2021). An open-source low-cost sensor for SNR-based GNSS reflectometry: design and long-term validation towards sea-level altimetry. *GPS Solutions*, *25*(2), 1-11.

Geremia-Nievinski, F., Hobiger, T., Haas, R., Liu, W., Strandberg, J., Tabibi, S., Vey, S., Wickert, J., & Williams, S. (2020). SNR-based GNSS reflectometry for coastal sea-level altimetry: Results from the first IAG inter-comparison campaign. *Journal of Geodesy*, 94(8), 70.

Gill, S. K., and T. N. Mero. 1990. Next generation water level measurement system: Implementation into the NOAA National Water Level Observation Network. In Towards an integrated system for measuring long term changes in global sea level, ed. H. F. Eden, Report of a workshop held at Woods Hole Oceanographic Institution, May 1990, pp. 133-146. Washington, DC: Joint Oceanographic Institutions Inc. (JOI).

Hannah, D. M., Demuth, S., van Lanen, H. A., Looser, U., Prudhomme, C., Rees, G., ... & Tallaksen, L. M. (2011). Large-scale river flow archives: importance, current status and future needs. *Hydrological Processes*, *25*(7), 1191-1200.

Holden, L. D., & Larson, K. M. (2021). Ten years of Lake Taupō surface height estimates using the GNSS interferometric reflectometry. *Journal of Geodesy*, *95*(7), 1-12.

IOC. (2006). *Manual on sea level measurement and interpretation, volume IV: an update to 2006* (IOC Manuals and Guides No.14, vol. IV; JCOMM Technical Report No. 31; WMO/ TD. No. 1339; p. 78). Intergovernmental Oceanographic Commission of UNESCO.

Jankowski, K. L., Törnqvist, T. E., & Fernandes, A. M. (2017). Vulnerability of Louisiana's coastal wetlands to present-day rates of relative sea-level rise. *Nature Communications*, *8*(1), 1-7.

Karegar, M. A., & Kusche, J. (2020). Imprints of COVID-19 lockdown on GNSS observations: An initial demonstration using GNSS interferometric reflectometry. *Geophysical research letters*, *47*(19), e2020GL089647.

Karegar, M. A., Larson, K. M., Kusche, J., & Dixon, T. H. (2020). Novel quantification of shallow sediment compaction by GPS interferometric reflectometry and implications for flood susceptibility. *Geophysical Research Letters*, *47*(14), e2020GL087807.

Keogh, M. E., & Törnqvist, T. E. (2019). Measuring rates of present-day relative sea-level rise in low-elevation coastal zones: a critical evaluation. *Ocean Science*, *15*(1), 61-73.

Knight, P. J., Bird, C. O., Sinclair, A., & Plater, A. J. (2020). A low-cost GNSS buoy platform for measuring coastal sea levels. *Ocean Engineering*, *203*, 107198.

Knight, P., Bird, C., Sinclair, A., Higham, J., & Plater, A. (2021). Testing an "IoT" Tide Gauge Network for Coastal Monitoring. *IoT*, *2*(1), 17-32.

Larson, K. M., & Nievinski, F. G. (2013). GPS snow sensing: results from the EarthScope Plate Boundary Observatory. *GPS solutions*, *17*(1), 41-52.

Larson, K. M., Braun, J. J., Small, E. E., Zavorotny, V. U., Gutmann, E. D., & Bilich, A. L. (2009). GPS multipath and its relation to near-surface soil moisture content. *IEEE Journal of Selected Topics in Applied Earth Observations and Remote Sensing*, *3*(1), 91-99.

Larson, K. M., Löfgren, J. S., & Haas, R. (2013). Coastal sea level measurements using a single geodetic GPS receiver. *Advances in Space Research*, *51*(8), 1301-1310.

Larson, K. M., Ray, R. D., Nievinski, F. G., & Freymueller, J. T. (2013). The accidental tide gauge: a GPS reflection case study from Kachemak Bay, Alaska. *IEEE Geoscience and Remote Sensing Letters*, *10*(5), 1200-1204.

Larson, K. M. (2021). kristinemlarson/gnssrefl: First release (1.0.10). Zenodo. https://doi.org/10.5281/zenodo.5601495

Löfgren, J. S., Haas, R., Scherneck, H. G., & Bos, M. S. (2011). Three months of local sea level derived from reflected GNSS signals. *Radio Science*, *46*(6).

Löfgren, J. S., Haas, R., & Scherneck, H. G. (2014). Sea level time series and ocean tide analysis from multipath signals at five GPS sites in different parts of the world. *Journal of Geodynamics*, *80*, 66-80.
Lyman, T. P., Elsmore, K., Gaylord, B., Byrnes, J. E., & Miller, L. P. (2020). Open Wave Height Logger: An open source pressure sensor data logger for wave measurement. *Limnology and Oceanography: Methods*, *18*(7), 335-345.
Mao, F., Khamis, K., Clark, J., Krause, S., Buytaert, W., Ochoa-Tocachi, B. F., & Hannah, D. M. (2020). Moving beyond the technology: a socio-technical roadmap for low-cost water sensor network applications. *Environmental Science & Technology*, *54*(15), 9145-9158.
Martin, C. R., Zeng, N., Karion, A., Dickerson, R. R., Ren, X., Turpie, B. N., & Weber, K. J. (2017). Evaluation and environmental correction of ambient CO 2 measurements from a low-cost NDIR sensor. *Atmospheric measurement techniques*, *10*(7), 2383-2395.
Nievinski, F. G., & Larson, K. M. (2014). Forward modeling of GPS multipath for near-surface reflectometry and positioning applications. *GPS solutions*, *18*(2), 309-322.
NMEA. (2018). *NMEA 0183 Interface Standard (Version 4.11).* National Marine Electronics Association. https://www.nmea.org/content/STANDARDS/NMEA_0183_Standard
Noye, B. J. 1974a. Tide-well systems I: Some non-linear effects of the conventional tide well. J. Mar. Res. 32(2): 129-135.
Paul, J. D., Buytaert, W., & Sah, N. (2020). A technical evaluation of lidar-based measurement of river water levels. *Water Resources Research*, *56*(4), e2019WR026810.
Penna, N. T., Morales Maqueda, M. A., Martin, I., Guo, J., & Foden, P. R. (2018). Sea surface height measurement using a GNSS Wave Glider. *Geophysical Research Letters*, 45, 5609–5616.
Pugh, D. T. 1972. The physics of pneumatic tide gauges. Int. Hydrogr. Rev. 49(2): 71-97.
Purnell, D. J., Gomez, N., Minarik, W., Porter, D., & Langston, G. (2021). Precise water level measurements using low-cost GNSS antenna arrays. *Earth Surface Dynamics*, *9*(3), 673-685.
Reid, A. J., Carlson, A. K., Creed, I. F., Eliason, E. J., Gell, P. A., Johnson, P. T., ... & Cooke, S. J. (2019). Emerging threats and persistent conservation challenges for freshwater biodiversity. *Biological Reviews*, *94*(3), 849-873.
Reinking, J., Roggenbuck, O., & Even-Tzur, G. (2019). Estimating wave direction using terrestrial GNSS reflectometry. *Remote Sensing*, *11*(9), 1027.
Rodrigues, F. S., & Moraes, A. O. (2019). ScintPi: A low-cost, easy-to-build GPS ionospheric scintillation monitor for DASI studies of space weather, education, and citizen science initiatives. *Earth and Space Science*, *6*(8), 1547-1560.
Roesler, C., & Larson, K. M. (2018). Software tools for GNSS interferometric reflectometry (GNSS-IR). *GPS solutions*, *22*(3), 1-10.
Roggenbuck, O., & Reinking, J. (2019). Sea surface heights retrieval from ship-based measurements assisted by GNSS signal reflections. *Marine Geodesy*, *42*(1), 1-24.
Roussel, N., Ramillien, G., Frappart, F., Darrozes, J., Gay, A., Biancale, R., ... & Allain, D. (2015). Sea level monitoring and sea state estimate using a single geodetic receiver. *Remote sensing of Environment*, *171*, 261-277.
Ruhi, A., Messager, M. L., & Olden, J. D. (2018). Tracking the pulse of the Earth's fresh waters. *Nature Sustainability*, *1*(4), 198-203.

Ruhi, A., Olden, J. D., & Sabo, J. L. (2016). Declining streamflow induces collapse and replacement of native fish in the American Southwest. *Frontiers in Ecology and the Environment*, *14*(9), 465-472.

Santamaría-Gómez, A., & Watson, C. (2017). Remote leveling of tide gauges using GNSS reflectometry: case study at Spring Bay, Australia. *GPS solutions*, *21*(2), 451-459.

Strandberg, J., Hobiger, T., & Haas, R. (2016). Improving GNSS-R sea level determination through inverse modeling of SNR data. *Radio Science*, *51*(8), 1286-1296.

Strandberg, J., Hobiger, T., & Haas, R. (2019). Real-time sea-level monitoring using Kalman filtering of GNSS-R data. *GPS Solutions*, *23*(3), 1-12.

Tranquilla, J. M., Carr, J. P., & Al-Rizzo, H. M. (1994). Analysis of a choke ring groundplane for multipath control in global positioning system (GPS) applications. *IEEE Transactions on antennas and propagation*, *42*(7), 905-911.

Williams, S. D., Bell, P. S., McCann, D. L., Cooke, R., & Sams, C. (2020). Demonstrating the potential of low-cost GPS units for the remote measurement of tides and water levels using interferometric reflectometry. *Journal of Atmospheric and Oceanic Technology*, *37*(10), 1925-1935.

Woodworth, P. L., & Smith, D. E. (2003). A one year comparison of radar and bubbler tide gauges at Liverpool. *The International hydrographic review*.